Int. J. Nonlinear Anal. Appl. 13 (2022) 2, 691–708
ISSN: 2008-6822 (electronic)
http://dx.doi.org/10.22075/ijnaa.2022.6464

Knee meniscus segmentation and tear detection based on magnitic resonacis images: A review of literature

Ali A. Mahdi*, Mohammed S.H. Al-Tamimi

Department of Computer Science, College of Science, University of Baghdad, Iraq

(Communicated by Madjid Eshaghi Gordji)

Abstract

The meniscus has a crucial function in human anatomy, and Magnetic Resonance Imaging (M.R.I.) plays an essential role in meniscus assessment. It is difficult to identify cartilage lesions using typical image processing approaches because the M.R.I. data is so diverse. An M.R.I. data sequence comprises numerous images, and the attributes area we are searching for may differ from each image in the series. Therefore, feature extraction gets more complicated, hence specifically, traditional image processing becomes very complex. In traditional image processing, a human tells a computer what should be there, but a deep learning (D.L.) algorithm extracts the features of what is already there automatically. The surface changes become valuable when diagnosing a tissue sample. Small, unnoticeable changes in pixel density may indicate the beginning of cancer or tear tissue in the early stages. These details even expert pathologists might miss. Artificial intelligence (A.I.) and D.L. revolutionized radiology by enhancing efficiency and accuracy of both interpretative and non-interpretive jobs. When you look at AI applications, you should think about how they might work. Convolutional Neural Network (C.N.N.) is a part of D.L. that can be used to diagnose knee problems. There are existing algorithms that can detect and categorize cartilage lesions, meniscus tears on M.R.I., offer an automated quantitative evaluation of healing, and forecast who is most likely to have recurring meniscus tears based on radiographs.

Keywords: Magnetic Resonance Imaging (M.R.I.), Convolutional Neural Network (C.N.N.), Deep learning (D.L.), Musculoskeletal (M.S.K.), Knee, Meniscus, Tear, Area Under the Curve (A.U.C.)
2020 MSC: 68T07

1 Introduction

Knee discomfort and damage are common in clinical practice. Approximately 2.5 million emergency department visits are attributed to sports-related knee injuries each year [20], and physicians are increasingly based on the results of musculoskeletal (M.S.K.) examinations imaging to aid diagnosis and therapy. [24] Even when interpreted by subspecialty trained M.S.K. radiologists, advanced M.S.K. imaging interpretation is labor-intensive and sensitive to reader variability, which may be ascribed to the huge amount of data given by each research and the tier of imaging particulars. D.L. algorithms incorporated into M.S.K. radiology workflows have the ability to improve diagnosis accuracy, speed up cases with critical findings, minimize tiredness for reader, and assist in decision-making in instances when radiological knowledge is lacking [4]. The majority of AI research on diagnosing knee pathology has focused on

*Corresponding author
Email addresses: ali.mqz@gmail.com (Ali A. Mahdi), m_altamimi75@yahoo.com (Mohammed S.H. Al-Tamimi)

Received: February 2022 *Accepted:* April 2022

creating C.N.N.s designed to perform interpretive jobs in the fields of pathology detection (cartilage lesion, meniscus torn), classification (assign osteoarthritis scores to knee radiographs, meniscus tears classification and segmentation (Figure 1).

Figure 1: Interpretive applications of D.L.(C.N.N.) in the evaluation of knee pathology [21].

C.N.N.s are a kind of D.L., a subclass of machine learning (M.L.) it denotes to algorithms with several interconnected layers similar of the layered technique employed by neurons in the brain [28]. C.N.N.s are a type of D.L. method that uses a mathematical process termed convolution, and they're used for image categorization and analysis (Figure 2). C.N.N. architecture is made up of a series of layers that, using a differentiable function, convert the input volume into an output volume (e.g., holding the class scores). There are several different sorts of layers that are often used. The convolutional layer is the most important parts of C.N.N.. The layer's parameters are made up of a set of learnable filters (or kernels) They have a narrow perceptron but cover the entire depth volume of the input.

Advances are being made using D.L. to accelerate M.R.I. acquisition. Regarding image-based tasks used to evaluate knee pathology after the acquisition of an image, C.N.N. currently has the greatest feasible to impacting lesion discover, characterization, and disease observing (Figure 3).

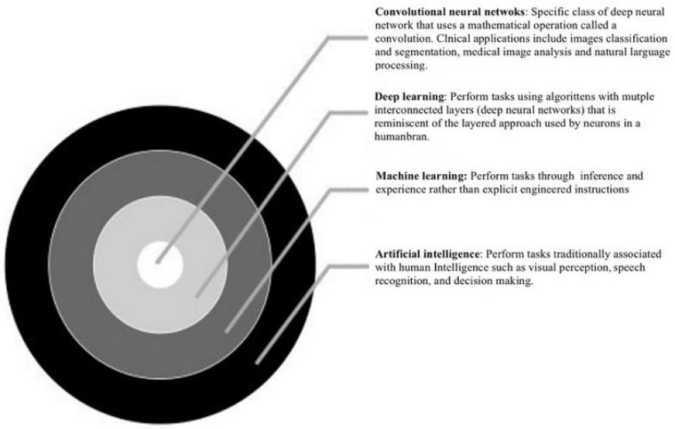

Figure 2: declarations outline of C.N.N.s [21].

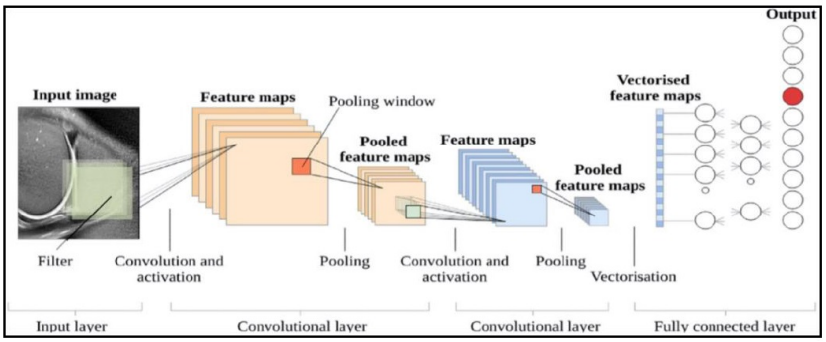

Figure 3: The impact of D.L. on image-based tasks used to evaluate knee pathology [21].

2 Magnetic resonance image

Magnetic resonance imaging (M.R.I.) is a radiographic technique used in radiology to create images of human body components. The brain, cartilages, spinal cord, bones and meniscus, the heart, and other internal organs are all imaged using M.R.I., which was produced with the use of massive and strong magnets. M.R.I. scanning is a method of generating three-dimensional reconstructions from several two-dimensional cross-sections or "slices" of tissue. M.R.I. scans are frequently made in three different orientations or planes, namely from the side (sagittal plane), the front (coronal plane), and the top-down (coronal plane) (axial plane). These planes are graphically shown in Figure 4. Three-dimensional M.R.I.s are thus a more difficult method of diagnostic imaging than two-dimensional X-rays.

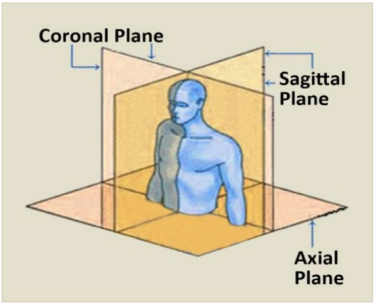

Figure 4: M.R.I. Image Reconstruction Planes [6]

2.1 M.I.R. Meniscus

M.R.I. is best suitable for achieving the desired result in the imaging diagnosis of meniscus tear and degeneration for several decades. The knee meniscus is a soft fiber kind of tissue present in between the femoral condyles and the tibial plateau, as shown in Figure 5.

Figure 5: Knee Meniscus [6]

2.2 M.R. image characteristic of knee

Musculoskeletal (M.S.K.) imaging is a sub-specialty in clinical radiology coping with diagnosing diseases related to bones and soft tissues. Different imaging modalities are used in M.S.K. radiology, including computed-tomography (C.T.), M.R.I., and Ultrasound. When various imaging modalities are available, M.R.I. is frequently selected due to its superior capacity to provide excellent soft tissue, meniscus contrast and its radiation-free nature [35]. Radiologists review scans for diagnostic reasons by imaging joints in various body areas such as the knee, hip, and shoulders, as well as tissues such as bone and muscle, monitoring the peripheral nervous system, and doing whole-body imaging to identify metabolic, aging, and other conditions. With enhanced imaging sequences and accompanying computational methods, the spectrum of clinical diagnoses that may be made with these radiology images is growing [25]. Knee M.R.I. is the most widely used M.S.K. radiology application because it has the most potential for accurately detecting abnormalities in the knee region [4]. Knee M.R.I. can identify a variety of abnormalities, including meniscus and cruciate pathology, as well as cartilage [43]. The number of scans and information given inside a knee M.R.I. fuel the necessity for developing automated analysis methodologies in such clinical applications (Figure 6).

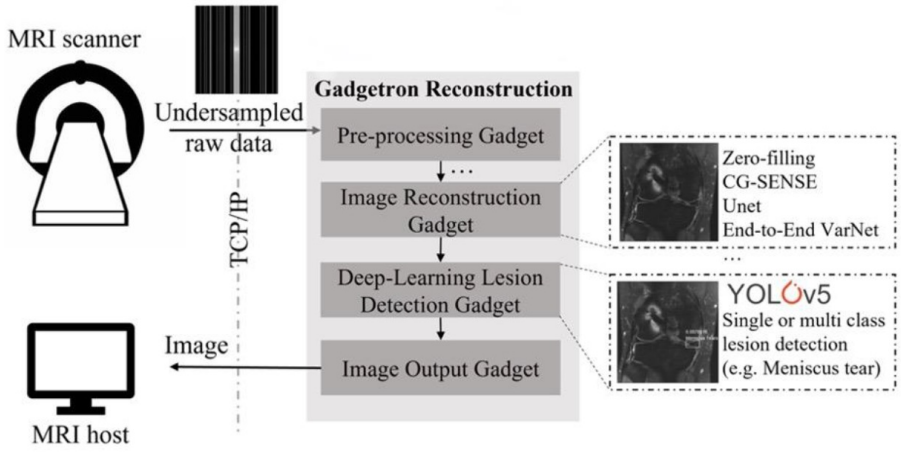

Figure 6: General flowchart for tear detection pipeline [63]

2.3 M.R.I. dataset of Knee Meniscus

We used a standard available dataset, contain multi-view knee M.R.I.s. The researchers used the examined dataset and categorized it as healthy or tears, which helped build a D.L. model that give robust results.

- MRNet dataset.
- Fast M.R.I. dataset.
- The Osteoarthritis Initiative (O.A.I.).

2.3.1 MRNet data set

The Stanford University Medical Center in Palo Alto, California, provided the MRNet with 1,370 M.R.I. exams of the knee and image size (255×255). The dataset contains 1,104 (80.6 percent) abnormal exams, Through manual extraction from clinical data, labels for 319 (23.3 percent) A.C.L. tears and 508 (37.1 percent) meniscus tears were acquired [1, 4, 29, 58] (Figure 7).

2.3.2 FastM.R.I. dataset

On 3 and 1.5 Tesla magnets, over 1,500 completely sampled knee M.R.I.s were acquired, as well as DICOM pictures (320×320) from 10,000 clinical knee M.R.I.s acquired on the same magnets. Coronal proton density-weighted images with and without fat suppression are included in the raw dataset. Axial proton density-weighted images with fat suppression, coronal proton density-weighted images with and without fat suppression, sagittal proton density, and sagittal T2-weighted images with fat suppression are all included in the DICOM collection [63].

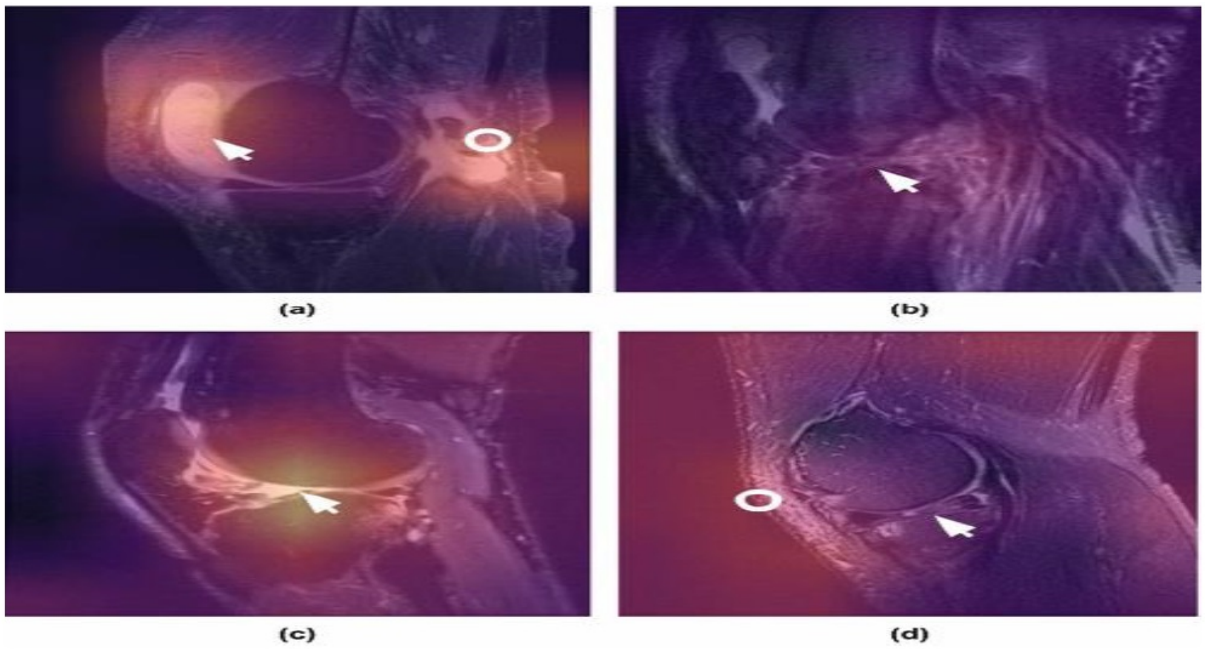

Figure 7: MRNet dataset [4]

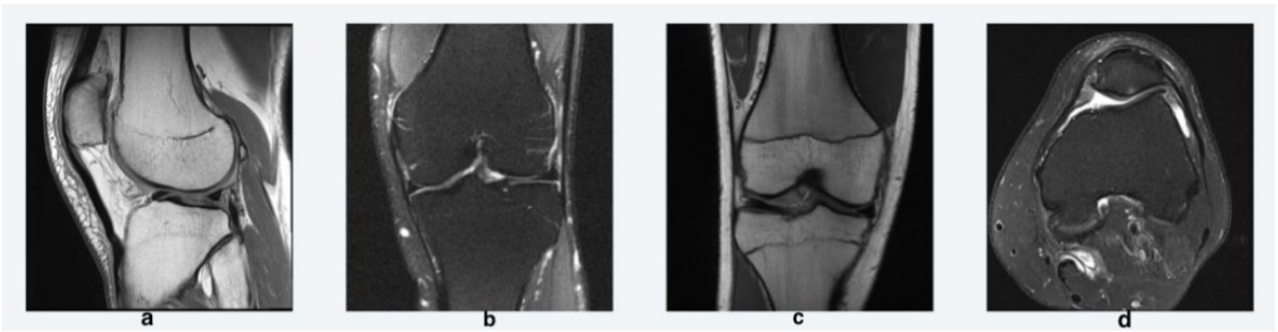

Figure 8: FastM.R.I. dataset in different position; image 'a' from the side of Knee, image 'b' from the back of Knee, image 'c' from front of Knee and image 'd' decleare the medial meniscus of Knee; from different patient [61]

2.3.3 The Osteoarthritis Initiative (O.A.I.)

Its massive database from an observational study of males and females over a 10 year period conducted across many centers. It contains data approximately 431,000 medical imaging visits and 26,626,000 M.R.I. and X-Ray images and different image size(from 128×128 to 256×256) [42, 50, 52].

3 Evaluation Metrics

This section discusses the evaluation processes to validate the performance of the meniscus stripping techniques and methods. The validation of meniscus stripping in term of quantitative measure.Quantitative is measurement of data that can be put into numbers. It is based on mathematical modeling, it used to run statistical analysis, so data has to be in numerical form. there are many measurement tools which used for the performance evaluation like :

3.1 Dice similarity index (D.S.I.)

Dice was the first to introduce the D.S.I., which is currently extensively used as a volume-based criterion for segmentation accuracy. Sometimes referred to as the Zijdenbos similarity index (ZSI) [56]. D.S.I. defined as:

$$S = \frac{2 \times |A \cap M|}{|A| + |M|} \times 100\%$$

Figure 9: Osteoarthritis image 'a' from the side of Knee, image 'b' from the front of Knee and image 'c' from side with zoom to decleare cartilages of Knee from different patient [**?**]

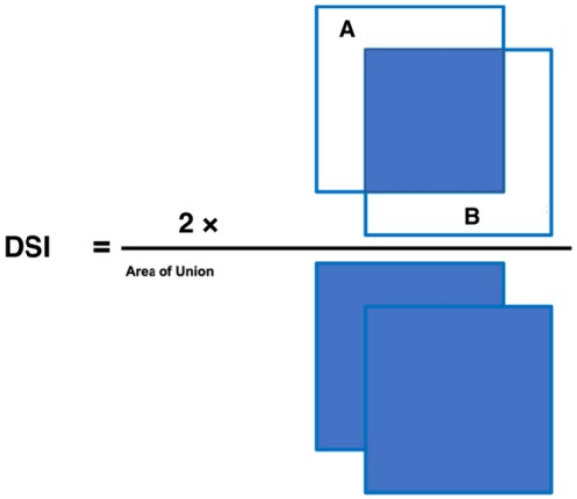

Figure 10: Explain Dice Similarity Index [2]

3.2 Dice similarity coefficient (D.S.C.) and sensitivity and specificity

It's the most often used benchmarks for metrics validation in knee joint segmentation architectures and tear detection processes are dice, sensitivity and specificity [57]. The following steps are used in performance assessment routines:

Dice similarity coefficient (D.S.C.): it is preventing the imbalance issue by focusing on local regions when segmentation the meniscus.

$$D.S.C. = \frac{2 \times T.P.}{2T.P. + F.P. + F.N.} \times 100\%$$

Sensitivity: the ability of a test to correctly identify M.R.I. with meniscus.

$$Sensitivity = \frac{T.P.}{T.P. + F.N.} \times 100\%$$

Specificity: the ability of a test to correctly identify M.R.I. without the meniscus.

$$Specificity = \frac{T.N.}{T.N. + F.P.} \times 100\%$$

WE can think of the true-positives (T.P.) and false-positives (F.P.), and false-negatives (F.N.) and true-negatives (T.N.) used in this way.

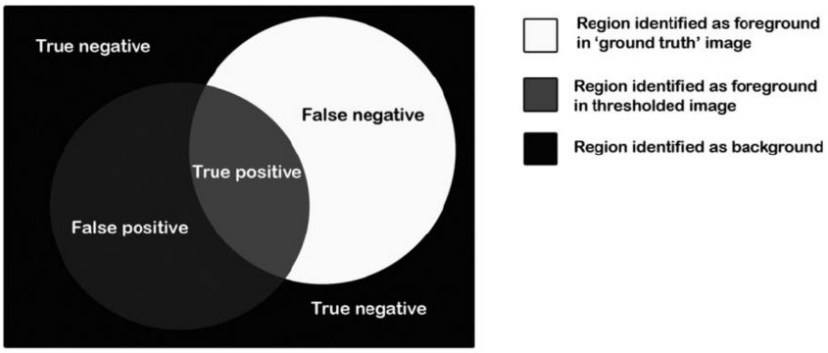

Figure 11: Explain Dice Similarity Coefficient (D.S.C.) [32]

3.3 Hausdorff Distance and average surface distance Measurement

They determine the distance between two surfaces' segmentation boundaries.

Hausdorff Distance:

$$\max(H(e_S, e_F), H(e_S, e_F)),$$

$$H(e_S, e_F) = \max_{d_i \in e_S} \left\{ \min_{d_j \in e_F} dist(d_i, d_j) \right\}$$

average surface distance:

$$\frac{1}{2}\left(\frac{\sum_{d_i \in e_S} \min_{d_j \in e_F} dist(d_i, d_j)}{\sum_{d_i \in e_S} 1} + \frac{\sum_{d_j \in e_F} \min_{d_i \in e_S} dist(d_j, d_i)}{\sum_{d_j \in e_F} 1} \right)$$

Where S =Segmentation of ground truth; F =Segmentation automatically; V =Size of volume; e_S =Ground-truth segmentation surfaces; e_F =Automatic segmentation surface; d_i =Surfaces vertices e_S, d_j =Surfaces vertices on the e_F; $dist(d_i, d_j)$= Euclidean distance among vertices d_i and d_j.

Hausdorff distance is the Max of all distances between voxels in Point 1 and their nearest voxels in Point 2, and vice versa.

when we takes the distances from the voxels of the gold standard mask to their nearest voxel in segmentation, and then it takes those distances and adds them together. This is called the average surface distance.

3.4 Receiver operating characteristic curve (R.O.C.)

At each classification threshold, a R.O.C. (receiver operating characteristic) curve can be seen. This graph illustrates the performance of classification model does at each threshold. This two parameters of curve plots:

- Rate of True Positive.
- Rate of False Positive.

True Positive Rate (T.P.R.) is a word for recall and hence has the following definition:

$$T.P.R. = \frac{T.P.}{T.P. + F.N.}$$

False Positive Rate (F.P.R.) has the following definition:

$$F.P.R. = \frac{F.P.}{F.P. + T.N.}$$

T.P.R. vs. F.P.R. at various classification thresholds is plotted on a R.O.C. curve. When classification threshold is lowered, more items are classified as positive, resulting in an increase in both False Positives and True Positives. A typical R.O.C. curve is shown in Figure 12.

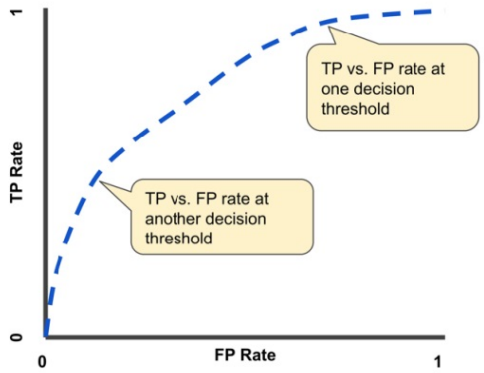

Figure 12: Rates of T.P. vs. F.P. at various classification threshold [**?**]

We might evaluate a logistic regression model multiple times with different classification thresholds to compute the points on a R.O.C. curve, but this would be inefficient. Fortunately, there is a fast, sorting-based algorithm called A.U.C. that can give us with this information.

3.5 Area Under the R.O.C. Curve

A.U.C. indicates "Area under the R.O.C. Curve". A.U.C. is a two-dimensional measurement of the complete lower portion the entire R.O.C. curve from (0,0) to (1,1) Figure 13.

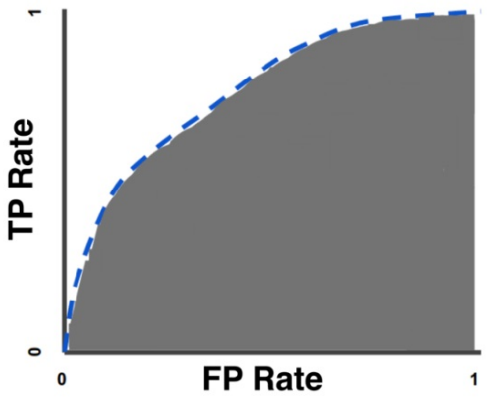

Figure 13: A.U.C. [**?**]

A.U.C. is a total measure of performance that takes into account whole forecasts classification thresholds. The likelihood that the model ranks a random positive example higher than a random negative example is one approach to analyze A.U.C.. For the following cases, which are listed in ascending order of logistic regression predictions from left to right:

The probability of a random positive (green) example being positioned to the right of a random negative (red) example is represented by the A.U.C..

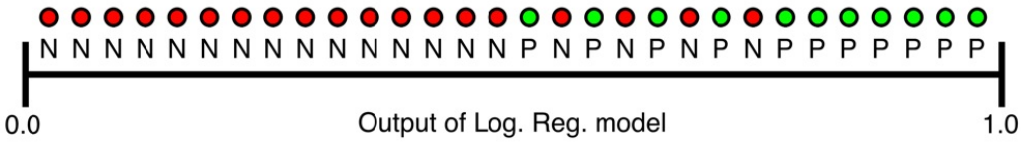

Figure 14: Forecasts are ranked by their logistic regression score in ascending order [**?**]

The A.U.C. value varies from 0 to 1. The A.U.C. of a model whose forecasts are 100 percent incorrect is 0.0, whereas the A.U.C. of a model whose forecasts are 100 percent right is 1.0.

For the 2 main reasons, A.U.C. is beneficial:

A.U.C. is scale-invariant: Rather of measuring absolute values, it assesses how well predictions are ordered.

A.U.C. is classification-threshold-invariant: It assesses the accuracy of the model's forecasts regardless of the categorization threshold used.

Both of these arguments, however, come with restrictions that may reduce A.U.C.'s utility in specific situations:

Scale invariance is not always desirable: For illustration, there are situations when we truly require finely calibrated probability outputs, which A.U.C. does not indicate.

Classification-threshold invariance is not always the best option. In circumstances where the cost of F.N vs. F.P is significantly different, it may be crucial to limit one form of classification error.

4 Related Work

4.1 Deep Learning

D.L. has several advantages over traditional M.L. methods [5], including the ability to automatically learn features at various abstraction levels using high-level classification objective functions [3] and the ability to design "end-to-end" methodologies in which the system can learn how to extract image features, detect and segment visual objects of interest, and classify the scene using a unified classification model [15]. The main challenge with D.L. models are the large number of parameters that must be estimated through the training process, necessitating an equally big, explanation training set in order to create stable training process. Due to the scarcity of large, annotated training sets, this problem is especially acute in medical-image-analysis (MIA) applications. In reality, the biggest MIA datasets often include tens of thousands of samples, which is widely regarded insufficient for successful D.L. model training. Mitosis detection and lymph node detection are two examples of early, successful MIA applications that used huge, annotated training sets [12, 47]. However, MIA issues with limited training sets have typically been addressed using regularization techniques such as unsupervised training [9, 14, 17, 33]. Deep auto-encoders have also been used to assess the utilization of registered multi-view input data [8, 23], which is identical to our methods excluding that our multi-view data is not commensurate. freshly, there was a surge of attention in developing D.L. methods for mammography analysis, which can be separated into three phases [22]:

- Tears detection (i.e., microcalcifications and aggregates).
- Segmentation of tears detected in the first stage.
- Tears are classified dependently textile and form features extracted from segmented tears.

Roblot et al. (2019) [46] presented D.L. assisted method to diagnosis knee (whole joint) using patients M.R.I and labeled by authors, the collected dataset 1123 images to train. 700 images training and get accuracy 83 percent, with D.L. architecture faster C.N.N..

Lassau N et al. (2019) [31] worked to find meniscus tear using M.R.I. datasets (collected from web not standard and labeled by team of researchers) depended on C.N.N.(AlexNet architecture); the study training 252 images then reported the best tested case 700 images and validation is 871 cases. The study accuracy 86 percent for A.C.L.(anterior cruciate ligament) tear and 72 percent for meniscus tear, the A.U.C. was 91 percent for meniscus tear.

Pedoia et al. (2019) [39] refer in their study to trained C.N.N.s(DenseNet architecture) to diagnose OA from T2 voxel based relaxometry data, analyzed for 4384 images from OAI dataset. D.L. outperformed shallow classifier. D.L. have A.U.C. 83.44 percent with accuracy 75 percent, shallow is A.U.C. 77.77 percent.

Pranata et al. (2019) [41] utilized C.N.N. base on Resnet and VGG architecture and attained Accuracy 98 percent in automated classification and detection of fractures using CT images; the method used speeded-up robust features (SURF), Canny edge detection and contour tracing. The datasets took from two sets of patient calcaneus bone of CT images, the first dataset have 987 images, the second dataset contain 944 images.

Urakawa et al. (2019) [59] used C.N.N. (VGG_16 architecture) to pre-trained model and transfer learning for outperformed orthopedic surgeons at detecting intertrochanteric fractures, obtained accuracy 95 percent using surgical registry database(dataset) have 1773 CT-images for patients.

Ho et al. (2019) [11] localization and find of hip fractures on PXRs (plain-frontal-pelvic-radiographs) by DC.N.N. (deep convolutional neural network), the dataset collected from 25,505 different limb radiograph views from 12,583 patients and they got accuracy 91 percent, A.U.C. 98 percent, sensitivity 98 percent, false negatives 2 percent.

Chang et al. (2019) [10] provides study aim on a simple C.N.N. (ResNet architecture) classifier for determining exist or not exist A.C.L. tear, the success validation accuracy is 76 percent from dataset contain 260 patients were included in the analysis, 130 of which had an A.C.L. tear and 130 of which were without A.C.L. tear.

Lu et al. (2018) [34] using C.N.N. (U-Net architecture) and NLP (natural language processing) (Deep Spine) to detected lumbar vertebral segmentation, spinal stenosis automatically; they used a large dataset of 22796 non-contrast M.R.I. from 4075 patients' examinations by Massachusetts General Hospital (MGH) Department of Radiology. Spinal canal stenosis accuracy 80.4 percent.

Table 1: D.L. methods in medical images field.

	Dataset	**Algorithm**	**Aim**	**Success ratio**
Roblot et al. (2019) [46]	1123 images. Collected by authors	D.L. architecture faster C.N.N.	knee diagnosis	83%
Lassau N et al. (2019) [31]	MRNet dataset	C.N.N. (AlexNet architecture)	Meniscus tear	72%
			A.C.L. tear	86%
Pedoia et al. (2019) [39]	OAI dataset	C.N.N.s (DenseNet architecture)	Diagnose OA from T2 voxel	75%
Pranata et al. (2019) [41]	Two set of CT images. Collected by authors	C.N.N. (Resnet and VGG architecture)	detection of fractures	98%
Urakawa et al. (2019) [59]	surgical registry database	C.N.N. (VGG_16 architecture)	intertrochanteric fractures	95%
Ho et al. (2019) [11]	25,505 different limb radiographs. Collected by authors	DC.N.N.	localization and find of hip fractures on PXRs	91%
Chang et al. (2019) [10]	260 M.R.I. Collected by authors	C.N.N. (ResNet architecture)	A.C.L. tear	76%
Lu et al. (2018) [34]	22796 non-contrast M.R.I. Collected by MGH	C.N.N. (U-Net architecture) and NLP	lumbar vertebral segmentation, spinal stenosis	80.4%

4.2 Using M.R.I. in Meniscus Study

The fibrocartilaginous meniscus is frequently damaged, and the injury can lead to accelerated cartilage deterioration. With the growth in popularity of meniscus-preserving operations, the fibrocartilaginous meniscus is regularly addressed surgically [45, 64]. The recommended noninvasive approach for identifying meniscus tears with aberrant meniscus morphology and/or signal intensity (24). Diagnostic performance of M.R.I when interpreted by radiologists in terms of sensitivity and specificity is 93 percent and 88 percent for medial meniscus (MM) tears and 79 percent and 96 percent for the lateral meniscus (L.M.) [36]. many computer-aided revealed approaches employing tissue analytical and/or supervised image classifiers have been described in the literatures, indicating a longstanding attention in auto-segmentation and diagnosis of meniscus tears [7, 19, 30, 44, 50, 60]. Table 2 lists and describes many innovative C.N.N.s for detecting and localizing meniscus disease.

Podolia et al. used the Whole-organ-Magnetic-Imaging-Score (WORMs) criteria to develop a 2-stage technique for bilateral identification of a meniscus "lesion" (current / truant) and severity assessment of that lesion (moderate vs highly) (31). For bilateral meniscus lesion unravel, C.N.N. reached a sensitivity of 80 percent and a privacy of 88 percent with area under the curve (A.U.C.) [26, 40] of 0.95, 0.84, and 0.89 on training, validation, and testing datasets consecutive.

Meniscus (crescent-shaped tissues between the tibia and femur bones) were classified as unharmed or tear using MRNet-dataset by Bien et al. [4], and C.N.N. performance was compared to that of radiologists. A radiologist harmony read on an interior authentication set of 120 examinations from the MRNet (1,370-examination items) became a standard reference.

Table 2: Surveys the performance of C.N.N.s in the unravel of meniscus torn [21].

Lesion	**Researcher**	**Reference standard**	**Sequence**	**Outcomes**	**Comments**
WORMs score meniscus lesions	Pedoia et a1. [39]	MSK radiologist read	Three-dimensional FSE CUBE	Sens: 81.98% spec: 89.81% A.U.C. 0.89	WORMS categorizes intrasubstance degeneration as a lesion
No tear (degenerative signal, postoperative, normal) vs tear	Bien et a1. [4]	MSK radiology consensus read on a subset	Sagittal T2 Coronal Tl Axial PD	A.U.C.: 0.847 Specificity: 0.741	Algorithm specificity for meniscus tear lower when compared with readers
Normal vs tear	Couteaux et al. [13]	Annotated data set	Sagittal T2 single image	Weighted A.U.C.: 0.906	Weighted A.U.C. included presence/absence of tear, orientation, and location
Normal vs tear	Roblot et al. [46]	Annotated data set	Sagittal T2 single image	A.U.C.: 0.94	Presence/absence of tear, orientation, and location were assessed

Couteaux et al. utilized a C.N.N.-based technique to categorized meniscus as "healthy" or "torn," as well as the direction and location of any tears that existed. This was done with the use of an annotated dataset of single sagittal M.R.I. that had been cropped to include the meniscus. For all three tasks, this method yielded a weighted A.U.C. of 90.6 percent (tear detection, orientation, and anatomical location) [13].

Roblot et al. [46] used the same C.N.N.-based approach to accomplish all three tasks on a bigger dataset and got a weighted A.U.C. of 90 percent.

4.3 Meniscus Segmentation Studies

In 1999, a first research in this field was completed [4]. In this research, segmentation was performed in two steps using fuzzy approaches on a relatively limited dataset (5 M.R.I.s), and the system's segmentation accuracy was not evaluated.

Fripp et al. [18] got the first remarkable outcome in segmentation terms, This study's beneficial elements include the success rates reached and the examination of both meniscus kinds (LM, MM). Although this study analyzed only healthy people, this circumstance is insignificant for studies aimed at providing help to radiology specialists.

Swanson et al. [56] segmented the lateral meniscus in M.R.I. images of the knee (OAI database) at both normal and negative levels. Average rates of success exceeding 80 percent for healthy images, 75 percent for level 0 images, 67 percent for level 1 images, and 64 percent for level 2 images were obtained in this investigation. The study's path should be determined by the poor success rate on sick photos. This was a study using semi-automated segmentation with a relatively tiny dataset (24 M.R.I.).

Swamy et al. [55] used thresholding and canny-edge-detection algorithms to sagittal segmentation, coronal, and planes axial on images of the meniscus collected by Scanners with a high field of view (3-Tesla) [55]. They manually commented on the segmented photographs, regardless of whether the images were torn or not. The study's segmentation on many planes might be seen as an advantage; the study not give number of M.R.I. used (size of dataset) and the number of healthy and torn and no success rate.

Zhang et al. [62] attained an 82 percent success rate despite the participants unknown health state [62]. The study's short comings include a lack of validation and a lack of information about the amount of M.R.I.(11 images as dataset) and Extreme learning machine, discriminative random fields methods was used. They performed four operations in separate serial excitation instead of assessment a single serial excitation in this investigation.

Table 3: Meniscus Segmentation Studies

Authors	**Meniscus Kind**	**Dataset**	**Health case**	**Algorithms**	**Success ratio (%)**
Fripp et al. (1999) [18]	M.M.	5 M.R.I.	Healthy	Active shape model.	77.10 ± 10.00
	L.M.				75.10 ± 10.00
Swanson et al. (2010) [56]	L.M.	24 M.R.I.	10 Healthy	Image filters, thresholding, region and shape limitations	80 (Control)
			14 Injured		75 (Level-0)
					67 (Level-1) 64 (Level-2)
Swamy et al. (2012) [55]	M.M.	Not Reported	Mixed	Thresholding, Canny edge detection	Not Reported
	L.M.				
Zhang et al. (2013) [62]	M.M.	11 M.R.I.	Not Reported	Discriminative random fields, extreme learning machine	82 ± 3
	L.M.				
Paproki et al. (2014) [37]	M.M.	88 M.R.I.	Mixed	Deformable model, template matching	75 ± 3
	L.M.				81 ± 2
Dam et al. (2015) [16]	M.M.	1907 M.R.I.	Mixed	Atlas-based method	76 ± 8
	L.M.				83 ± 5
Saygili et al. (2016) [51]	M.M.	88 M.R.I.	Mixed	HOG, tree bagging	91.009
Paproki et al. (2017) [38]	M.M.	80 M.R.I.	Mixed	Statistical shape model, template matching	76.4% 76.4%
	L.M.				84.3% 85.1%
					75.2% 76.1%
Tack et al. (2018) [54]	M.M.	88 M.R.I.	Mixed	Convolutional neural network, statistical shape model	80.87 ± 3.92
	L.M.				

Paproki et al. [37] successfully segmented both types of meniscuses [37].the success rate 75 percent in MM and 82 percent in LM. The dataset used from OAI (88 M.R.I.) and used deformable model approach to segmentation. The study's weakness can be attributed to the approximately 30 minutes required for segmentation(very long time).

One of the most noteworthy studies is that of Dam et al. [16] at three distinct sets of data with varied excitation serialization consisted of 1907 different M.R.I.s from OAI dataset and Atlas-based method to segmented meniscuses, they attained successful segmentation rate with 76 percent in M.M. and 83 percent in L.M., consecutive. Low- and high-resolution images were compared. The study was not assigned the number of healthy and injured in meniscuses M.R.I..

In 2016, Saygili et al. employed 88 M.R.I. (OAI dataset) to determine the best frames for meniscus [51]. They had a 91 percent success rate. Saygili et al. conducted study [49] that proposed a novel method for fully auto-detection of meniscus. Histogram of Oriented Gradients (H.O.G.) and Local Binary Pattern (L.B.P.) feature extraction techniques, Extreme Learning Machines (E.L.M.) and Random Forests (R.F.) classification techniques utilized in this study, that utilized morphological handles for the determination of the R.O.I.. This study attains successful segmentation rate 82.73 percent. The study's shortcoming is that the work is limited to the M.M. Additionally, this study's shortcomings include the fact that just the meniscus frames were collected, and not determined the boundaries of meniscus.

Paproki et al. [38] conducted segment of meniscus examine with statistical surface models (S.M.M.) compared auto analysis with manual analysis. Three different Patterns of image were utilized in this research. The average D.S.I.

valuable were 76 percent to Two-Dimensional Turbo Spin-Echo (2D-TSE) M.R.I., 84 percent for Three-Dimensional Turbo Spin-Echo (3D-TSE) M.R. images, 75 percent for T2 Maps, consecutive. The study's strengths include the utilization of M.R.Is acquired in many planes and the comparison of manual and automatic analysis. The study was said "All datasets used for analyses were anonymized"!, the number of healthy and injured in meniscuses M.R.I. are not given.

Tack et al. presented the first paper to segment meniscus structures using knee M.R.I.s in 2018 [54]. When the results of this study are analyzed, it is clear that the essential work done in this field will continue in the same path. With a total success rate of 80.87 percent, Tack's work used C.N.N.s. There are no assigned the number of healthy and injured in meniscuses M.R.I.. In this study.

4.4 Meniscus Tear Detection Studies

Meniscus segmentation research are used to detect tears in segmented images automatically. The detection of tears will assist radiology specialists in their work and decision-making.

Hata et al. Finished the initial study on the identification of meniscus torn in 2001 [27], which is an enhanced edition of the study [48] carried out in 1999. Although the torn has been identified in this task, the verification procedure has not been carried out. As a result, the system's efficiency cannot be guaranteed. There is a lack of information about the amount of M.R.I. and health case; and used multi-methods without success rate declared.

Boniatis et al. noted in their 2008 study they wished for establish a differentiation between healthy and injured meniscus [7]. Although the study appears to assess 55 separate M.R.I. from clinical observation, classification is based on 55 slice images involving the posterior meniscus horns, Although the success rate 89 percent appears to be powerful in Boniatis's work, reaching this successful rate with 55 slice images raises concerns about the study's generalizability.

Köse et al. designed an auto-approach for detecting meniscus tears on 500 M.R.I. dataset from Karadeniz Technical University [30]. The success rate for torn meniscus images is 88.3 percent, whereas the success rate for healthy images is 95.7 percent. However, the study contains numerous uncertainties. To begin, as in Boniatis's study, the study was conducted using by selected slices manually from M.R.I. [7]. In other words, instead of using 3D M.R. images, the study used 2D slices. It's also stated that 500 photos were taken from 30 different patients, however they are not used to their maximum potential. It's also been observed that diagnosing a torn meniscus requires more than 30 photos, whilst diagnosing a healthy one requires more than 70 images. Furthermore, there is no assessment of how M.R.I. slices are selected.

Ramakrishna et al. designed auto-computer-assisted diagnostic approach for M.R.I.s obtained using T1 excitation sequences from low field scanners. [44]. As an outcome of their work, they acquired a sensitivity amount is 83.87 percent and a specificity amount is 75.19 percent, 40 from archived database participants with varying levels of meniscus torn and Computer aided diagnosis (CAD) as a method, Their method has become highly reliant on their dataset. As a result, it is doubtful that this approach will be used to another dataset, the success rate not given.

Fu et al. employed active contour with level sets method for segmentation, then feature extraction with co-occurrence matrices, and lastly classification with SVM [19]. The huge set of data size of the study (166 M.R.I. unknown dataset) is a positive aspect. The capacity to find torn in a single image in 5.5 sec is most notable benefit of this work. The initial user-defined frames indicate that it is a semi-automatic approach, the success rate not given; only sensitivity is 72.7 percent.

The perfect outcome in meniscus tear detection experiments were reported by Zarandi et al. [60]. They used fuzzy-clustering algorithms for segmentation and used sensor neural networks for classification. A precision value of $88.82 - 92.13$ percent was found based on the meniscus type and region in this investigation, which was conducted on 50 patients M.R.I. (dataset) from clinical observation in MohebMehr Hospital have healthy and non-healthy meniscus. Using proton-weighted images, researchers were able to detect meniscus tears more accurately than with previous (T1 and T2) excitation sequences. About the detect more accurate came when study's used neural networks, the dataset very small was a lack.

Roblot et al. [46] presented D.L. assisted method to meniscus tear detection using patients M.R.I. and labeled by authors, the collected dataset 1123 images to train. 700 images training and get accuracy 83 percent, with faster C.N.N. architecture. The dataset used in this study not evaluated from other studies and not standard, the highly accuracy with faster C.N.N. needed to audit.

Lassau N et al. [53] worked to find meniscus tear using different M.R.I. datasets (collected from web not standard and labeled by team of researchers was leaked the study) depended on C.N.N.(AlexNet architecture); the study training

252 images then reported the best tested case 700 images and validation is 871 cases. The study accuracy 72 percent for meniscus tear, the A.U.C. was 91 percent for meniscus tear.

The C.N.N. (MRNet; 1130 M.R.I. training and 120 M.R.I. validation exams), Bien et al. described an area under curve (A.U.C.) of 84.7 percent and accuracy 72.5 percent for finding meniscus tears [4]. The study can increase the accuracy if change C.N.N. architecture not.

Meniscus tears have previously been researched to see if the meniscus is torn. Meniscus are categorized based on the type of tear that occurs (horizontal tears, vertical tears, etc.). Meniscus tear kinds will be studied further in the future, and this field will benefit much from it. Such conclusions produced with D.L. based methods, in particular, will make a significant contribution to the literature.

Table 4: meniscus tear studies

Author(s)	**Meniscus kind**	**Data Size**	**Health Status**	**Algorithm**	**Success Rate (%)**
Hata et al. [27]	Not Reported	NA	Mixed	multi-methods	NA
Boniatis et al. [7]	MM-Posterior Horn	55 M.R.I.	Mixed	multi-methods	89.1
Köse et al. [30]	Not Reported	500 M.R.I.	Mixed	designed an auto-approach	For wounded participants, accuracy was 88.3%. For healthy participants, the accuracy was 95.7 percent.
Ramakrishna et al. [44]	MM- Anterior and Posterior Horn LM- Anterior and Posterior Horn	40 M.R.I.	Injured	auto-computer-assisted	Sensitivity: 83.87 Specificity: 75.19
Fu et al. [19]	Not Reported	166 M.R.I.	Mixed	SVM	Sensitivity: 0.727
Zarandi et al. [60]	MM- Anterior and Posterior Horn LM- Anterior and Posterior Horn	50 M.R.I.	Mixed	neural networks	Precision: 88.82-92.13
Roblot et al. [46]	MM	1123 M.R.I.	Mixed	faster C.N.N.	83
Lassau N et al. [53]	LM	NA	Mixed	C.N.N. (AlexNet architecture);	72
Bien et al [4]	MM LM	MRNet	Mixed	C.N.N.	72.5

5 Conclusion

Meniscus and cartilage; its most important ingredient of the knee joint. Damage to the cartilage structures caused by a meniscus injury can lead to osteoarthritis. Furthermore, a torn meniscus limits one's capacity to move. As a result, early detection of meniscus tissues is critical in order to perform routine inspections quickly and with minimal error rates. Numerous research on meniscus segmentation and tear detection have been conducted over time for these objectives. The meniscus in the knee are complex to evaluate because they don't have separate forms. When physically evaluating these tissues, radiologists can make mistakes, and even if they don't, they lose a lot of time. The studies' objective is to build methods capable of reducing evaluation times and assisting radiology and orthopedic specialists in making decisions. The studies conducted in this field will become even more critical in the coming years. There are only a few studies on D.L. in this domain. Studies that identify tears based on their location will benefit this field and assist specialists in determining the type of meniscus tear. The development of D.L. will deliver a considerable boost. According to research, this automated detection system will be used in M.R.I. devices. There will be a significant decrease in the rate of misdiagnosis.

References

[1] D. Azcona, K. McGuinness and A.F. Smeaton, *A comparative study of existing and new deep learning methods for detecting knee injuries using the MRNet dataset*, Int. Conf. Intell. Data Sci. Technol. Appl. IDSTA 2020, pp. 149–155.

[2] M. Bardis, R. Houshyar, C. Chantaduly, A. Ushinsky, J. Glavis-Bloom, M. Shaver, D. Chow, E. Uchio and P. Chang, *Deep learning with limited data: Organ segmentation performance by U-Net*, Electron. **9** (2020), no. 8.

[3] Y. Bengio, *Learning deep architectures for AI, Found.*, Trends Mach. Learn. **2** (2009), no. 1.

[4] N. Bien P. Rajpurkar, R.L. Ball, J. Irvin, A. Park, E. Jones, M. Bereket, B.N. Patel, K.W. Yeom, K. Shpanskaya and S. Halabi, *Deep-learning-assisted diagnosis for knee magnetic resonance imaging: Development and retrospective validation of MRNet*, PLoS Medicine **15** (2018), no. 11, 1–19.

[5] C.M. Bishop and N.M. Nasrabadi, *Pattern recognition and machine learning*, New York, Springer, 2006.

[6] Boehringer-Ingelheim, *Radiology rounds; A closer look at interstitial lung disease*, Boehringer-Ingelheim Website, https://www.ipfradiologyrounds.com/hrct-primer/image-reconstruction/.

[7] I. Boniatis, G. Panayiotakis and E. Panagiotopoulos, *A computer-based system for the discrimination between normal and degenerated menisci from magnetic resonance images*, IEEE Int. Workshop Imag. Syst. Tech. IEEE, 2008, pp. 335–339.

[8] T. Brosch, Y. Yoo, D.K.B. Li, A. Traboulsee and R. Tam, *Modeling the variability in brain morphology and lesion distribution in multiple sclerosis by deep learning*, Int. Conf. Medical Image Comput. Computer-Assisted Intervention, 2014, pp. 462–469.

[9] G. Carneiro and J.C. Nascimento, *Combining multiple dynamic models and deep learning architectures for tracking the left ventricle endocardium in ultrasound data*, IEEE Trans. Pattern Anal. Mach. Intell. **35** (2013), no. 11, 2592–2607.

[10] P.D. Chang, T.T. Wong and M.J. Rasiej, *Deep learning for detection of complete anterior cruciate ligament tear*, J. Digital Imag. **32** (2019), no. 6, 980–986.

[11] C.-T. Cheng, T.-Y. Ho, T.-Y. Lee, C.-C. Chang, C.-C. Chou and C.-C. Chen, *Application of a deep learning algorithm for detection and visualization of hip fractures on plain pelvic radiographs*, Eur. Radiol. **29** (2019), no. 10, 5469–5477.

[12] D.C. Cireşan, A. Giusti, L.M. Gambardella and J. Schmidhuber, *Mitosis detection in breast cancer histology images with deep neural networks*, Int. Conf. Medical Image Computing and Computer-Assisted Intervention, Springer, Berlin, Heidelberg, 2013, pp. 411–418.

[13] V. Couteaux, S. Si-Mohamed, O. Nempont, T. Lefevre, A. Popoff, G. Pizaine, N. Villain, I. Bloch, A. Cotten and L. Boussel, *Automatic knee meniscus tear detection and orientation classification with Mask-RCNN*, Diagn. Intervent. Imag. **100** (2019), no. 4, 235–242.

[14] A.A. Cruz-Roa, J.E.A. Ovalle, A. Madabhushi and F.A.G. Osorio, *A deep learning architecture for image representation, visual interpretability and automated basal-cell carcinoma cancer detection*, Medical Image Computing and Computer-Assisted Intervention – MICCAI 2013, Springer, 2013, pp. 403–410.

[15] J. Dai, K. He and J. Sun, *Instance-aware semantic segmentation via multi-task network cascades*, Proc. IEEE Conf. Comput. Vis. Pattern Recogn. 2016, pp. 3150–3158.

[16] E.B. Dam, M. Lillholm, J. Marques and M. Nielsen, *Automatic segmentation of high- and low-field knee MRIs using knee image quantification with data from the osteoarthritis initiative*, J. Med. Imag. (Bellingham) **2** (2015), no. 2, 024001.

[17] R. Fakoor, F. Ladhak, A. Nazi and M. Huber, *Using deep learning to enhance cancer diagnosis and classification, In Proceedings of the Int. Conf. on machine learning*, ACM, New York, USA **28** (2013), 3937–3949.

[18] J. Fripp, P. Bourgeat, C. Engstrom, S. Ourselin, S. Crozier and O. Salvado, *Automated segmentation of the menisci from MR images*, IEEE Int. Symp. Biomed. Imag. From nano to macro, IEEE, 2009, pp. 510–513.

[19] J.-C. Fu, C.-C. Lin, C.-N. Wang and Y.-K. Ou, *Computer-aided diagnosis for knee meniscus tears in magnetic resonance imaging*, JIPE **30** (2013), no. 2, 67–77.

[20] B.E. Gage, N.M. McIlvain, C.L. Collins, S.K. Fields and R.D. Comstock, *Epidemiology of 6.6 million knee injuries presenting to United States emergency departments from 1999 through 2008*, Acad. Emerg. Med. **19** (2012), no. 4, 378–385.

[21] E.R. Garwood, R. Tai and G. Joshi, *The use of artificial intelligence in the evaluation of knee pathology*, Seminars in Musculoskeletal Radiology, 24 (2020), no. 1, 21–29.

[22] M.L. Giger, N. Karssemeijer and J.A. Schnabel, *Breast image analysis for risk assessment, detection, diagnosis, and treatment of cancer*, Annual Rev. Biomed. Eng. **15** (2013), 327–357.

[23] Y. Guo, G. Wu, L.A. Commander, S. Szary, V. Jewells, W. Lin and D. Shen, *Segmenting hippocampus from infant brains by sparse patch matching with deep-learned features*, Int. Conf. Med. Image Comput. Comput.-Ass. Interven. 2014, pp. 308–315.

[24] S. Gyftopoulos, P. Harkey, J. Hemingway, D.R. Hughes, A.B. Rosenkrantz and R.D. Jr, *Changing musculoskeletal extremity imaging utilization from 1994 through 2013: A medicare beneficiary perspective*, Amer. J. Roentg. **209** (2017), no. 05, 1103–1109.

[25] S. Gyftopoulos, D. Lin, F. Knoll, A.M. Doshi, T.C. Rodrigues and M.P. Recht, *Artificial intelligence in musculoskeletal imaging: Current status and future directions*, Amer. J. Roentg. **213** (2019), no. 3, 506.

[26] D.J. Hand and R.J. Till, *A simple generalization of the area under the ROC curve for multiple class classification problems*, Mach. Learn. **45** (2001), no. 2, 171–186.

[27] Y. Hata, S. Kobashi, Y. Tokimoto, M. Ishikawa and H. Ishikawa, *Computer aided diagnosis system of meniscal tears with T1 and T2 weighted MR images based on fuzzy inference computational intelligence theory and applications*, Int. Conf. Computat.Intell. 2001, pp. 55–58.

[28] A. Hosny, C. Parmar, J. Quackenbush, L.H. Schwartz and H.J.W.L. Aerts, *Artificial intelligence in radiology*, Nat. Rev. Cancer **18** (2018), no. 8, 500–510.

[29] I. Irmakci, S.M. Anwar, D.A. Torigian and U. Bagci, *Deep learning for musculoskeletal image analysis*, 53rd Asilomar Conf. Signals, Syst. Comput. IEEE, 2019, pp. 1481–1485.

[30] C. Köse, O. Gençalioğlu and U. Şevik, *An automatic diagnosis method for the knee meniscus tears in MR images*, Expert Syst. Appl. **36** (2009), no. 2, 1208–1216.

[31] N. Lassau, T. Estienne, P. de Vomecourt, M. Azoulay, J. Cagnol, G. Garcia, M. Majer, E. Jehanno, R. Renard-Penna, C. Balleyguier and F. Bidault, *Five simultaneous artificial intelligence data challenges on ultrasound, CT, and MRI*, Diagn. Interv. Imag. **100** (2019), no. 4, 199–209.

[32] E.A. Levin, R.M. Morgan, L.D. Griffin and V.J. Jones, *A comparison of thresholding methods for forensic reconstruction studies using fluorescent powder proxies for trace materials*, J. Forensic Sci. **64** (2019), no. 2, 431–442.

[33] R. Li, W. Zhang, H.I. Suk, L. Wang, J. Li, D. Shen and S. Ji, *Deep learning based imaging data completion for improved brain disease diagnosis*, Int. Conf. Medical Image Comput. Comput.-Ass. Interven. 2014, pp. 305–312.

[34] J.-T. Lu, S. Pedemonte, B. Bizzo, S. Doyle, K.P. Andriole and M.H. Michalski, *DeepSPINE: Automated lumbar vertebral segmentation, disc-level designation, and spinal stenosis grading using deep learning*, Machine Learn. Healthcare Conf. PMLR, 2018, pp. 403–419.

[35] N.C. Nacey, M.G. Geeslin, G.W. Miller and J.L. Pierce, *Magnetic resonance imaging of the knee: An overview and update of conventional and state of the art imaging*, Magnetic Resonance Imag. **45** (2017), no. 5, 1257–1275.

[36] J.C. Nguyen, A.A. De Smet, B.K. Graf and H.G. Rosas, *MR imaging-based diagnosis and classification of meniscal tears*, Radiograph. **34** (2014), no. 04, 981–999.

[37] A. Paproki, C. Engstrom, S.S. Chandra, A. Neubert, J. Fripp and S. Crozier, *Automated segmentation and analysis of normal and osteoarthritic knee menisci from magnetic resonance images–data from the osteoarthritis initiative*, Osteoarthritis Cartilage **22** (2014), no. 9, 1259–1270.

[38] A. Paproki, C. Engstrom and M. Strudwick, *Automated T2- mapping of the menisci from magnetic resonance images in patients with acute knee injury*, Acad. Radiol. **24** (2017), no. 10, 1295–1304.

[39] V. Pedoia, J. Lee, B. Norman, T.M. Link and S. Majumdar, *Diagnosing osteoarthritis from T2 maps using deep*

learning: An analysis of the entire osteoarthritis initiative baseline cohort, Osteoarthritis Cartilage **27** (2019), no. 7, 1002–1010.

[40] V. Pedoia, B. Norman, S.N. Mehany, M.D. Bucknor, T.M. Link and S. Majumdar, *3D convolutional neural networks for detection and severity staging of meniscus and PFJ cartilage morphological degenerative changes in osteoarthritis and anterior cruciate ligament subjects*, J. Magnetic Resonance Imag. **49** (2019), no. 2, 400–410.

[41] Y.D. Pranata, K.C. Wang, J.C. Wang, I. Idram, J.Y. Lai, J.W. Liu and I.H. Hsieh, *Deep learning and SURF for automated classification and detection of calcaneus fractures in CT images*, Comput.Meth. Prog. Biomed. **171** (2019), 27–37.

[42] M.M. Rahman, L. Dürselen and A.M. Seitz, *Automatic segmentation of knee menisci - A systematic review*, Artif. Intell. Med. **105** (2020), p. 101849.

[43] A. Raj, S. Vishwanathan, B. Ajani, K. Krishnan and H. Agarwal, *Automatic knee cartilage segmentation using fully volumetric convolutional neural networks for evaluation of osteoarthritis*, IEEE 15th Int. Symp. Biomed. Imag. (ISBI 2018), IEEE, 2018, pp. 851–854.

[44] B. Ramakrishna, W. Liu, G. Saiprasad, N. Safdar, C.I. Chang, K. Siddiqui, W. Kim, E. Siegel, J.W. Chai, C.C.C. Chen and S.K. Lee, *An automatic computer-aided detection system for meniscal tears on magnetic resonance images*, IEEE Trans. Med. Imag. **28** (2009), no. 8, 1308–1316.

[45] M.P. Recht and J. Kramer, *MR imaging of the postoperative knee: A pictorial essay*, Radiograph. **22** (2002), no. 4, 765–774.

[46] V. Roblot, Y. Giret and M.B. Antoun, *Artificial intelligence to diagnose meniscus tears on MRI*, Diagn. Interv. Imag. **100** (2019), no. 4, 243–249.

[47] H.R. Roth, L. Lu, A. Seff, K.M. Cherry, J. Hoffman, S. Wang, J. Liu, E. Turkbey and R.M. Summers, *A new 2.5 D representation for lymph node detection using random sets of deep convolutional neural network observations*, Int. Conf. Med. Image Comput. Comput.-Ass. Interv. 2014, pp. 520–527.

[48] T. Sasaki, Y. Hata, Y. Ando, M. Ishikawa and H. Ishikawa, *Fuzzy rule based approach to segment the menisci region from MR images*, In Medical Imaging 1999: Image Processing, Int. Soc. Opt. Photon. **3661** (1999), 258–265.

[49] A. Saygılı and S. Albayrak, *A new computer-based approach for fully automated segmentation of knee meniscus from magnetic resonance images*, Biocybern. Biomed. Eng. **37** (2017), no. 3, 432–425.

[50] A. Saygılı and S. Albayrak, *An efficient and fast computer-aided method for fully automated diagnosis of meniscal tears from magnetic resonance images*, Artif. Intell. Med. **97** (2019), no. 13, 118–130.

[51] A. Saygili, H. Kaya and S. Albayrak, *Automatic detection of meniscal area in the knee MR images*, Signal Process. Commun. Appl. Conf. (SIU), 2016, pp. 1337–1340.

[52] A. Saygılı and S. Varlı, *Automated diagnosis of meniscus tears from MRI of the knee*, Int.Sci. Vocat. Stud. J. **3** (2019), no. 2, 92–104.

[53] B. Schmauch, P. Herent, P. Jehanno, O. Dehaene, C. Saillard, C. Aubé, A. Luciani, N. Lassau and S. Jégou, *Diagnosis of focal liver lesions from ultrasound using deep learning*, Diagn. Intervent. Imag. **100** (2019), no. 4, 227–233.

[54] H. Seim, D. Kainmueller, H. Lamecker, M. Bindernagel, J. Malinowski and S. Zachow, *Model-based auto-segmentation of knee bones and cartilage in MRI data*, Proc. MICCAI Workshop Med. Image Anal. Clinic, 2010, pp. 215–223.

[55] M.S.M. Swamy and M.S. Holi, *Knee joint menisci visualization and detection of tears by image processing*, Int. Conf. Comput. Commun. Appl. ICCCA 2012, 2012, pp. 1–5.

[56] M.S. Swanson, J.W. Prescott and T.M. Best, *Semi-automated segmentation to assess the lateral meniscus in normal and osteoarthritic knees*, Osteoarthritis Cartilage **18** (2010), no. 3, 344–353.

[57] J.G. Tamez-Peña, S. Totterman and K.J. Parker, *Unsupervised statistical segmentation of multispectral volumetric MRI images*, Proc. SPIE **3661** (1999), 300–311.

[58] C.-H. Tsai, N. Kiryati, E. Konen, I. Eshed and A. Mayer, *Knee injury detection using MRI with efficiently-layered*

network (ELNet), Med. Imag. Deep Learn. PMLR, **2020** (2020), 784–794.

[59] T. Urakawa, Y. Tanaka, S. Goto, H. Matsuzawa, K. Watanabe and N. Endo, *Detecting intertrochanteric hip fractures with orthopedist-level accuracy using a deep convolutional neural network*, Skelet. Radiol. **48** (2019), no. 2, 239–244.

[60] M.H.F. Zarandi, A. Khadangi, F. Karimi and I.B. Turksen, *A computer-aided type-II fuzzy image processing for diagnosis of meniscus tear*, J. Digit. Imag. **29** (2016), no. 6, 677–695.

[61] J. Zbontar, F. Knoll, A. Sriram, T. Murrell, Z. Huang, M.J. Muckley, A. Defazio, R. Stern, P. Johnson, M. Bruno, M. Parente, K.J. Geras, J. Katsnelson, H. Chandarana, Z. Zhang, M. Drozdzal, A. Romero, M. Rabbat, P. Vincent, N. Yakubova, J. Pinkerton, D. Wang, E. Owens, C.L. Zitnick, M.P. Recht, D.K. Sodickson and Y.W. Lui, *fastMRI: An open dataset and benchmarks for accelerated MRI*, arXiv:1811.08839, (2019).

[62] K. Zhang, W. Lu and P. Marziliano, *The unified extreme learning machines and discriminative random fields for automatic knee cartilage and meniscus segmentation from multi-contrast MR images*, Mach. Vis. Appl. **24** (2013), no. 7, 1459–1472.

[63] R. Zhao, Y. Zhang, B. Yaman, M.P. Lungren and M.S. Hansen, *End-to-end AI-based MRI reconstruction and lesion detection pipeline for evaluation of deep learning image reconstruction*, arXiv preprint arXiv:2109.11524, (2021).

[64] B. Zikria, N. Hafezi-Nejad, F.W. Roemer, A. Guermazi and S. Demehri, *Meniscal surgery: Risk of radiographic joint space narrowing progression and subsequent knee replacement-data from the osteoarthritis initiative*, Radiol. **282** (2017), no. 3, 807–816.